IJRCS

International Journal of Robotics and Control Systems
Vol. 6, No. 2, 2026, pp. 1513-1530
ISSN 2775-2658
http://pubs2.ascee.org/index.php/ijrcs

ASCEE

FPGA Based Sensorless Sliding Mode Observer with Phase-Locked Loop for PMSM Drives: Design, Verification and Implementation

Nguyen Khanh Quang [a,1,*], Ha Duc Phi [a,2], Le Phu Vu [a,3], Phan Minh Tuan [a,4], Nguyen Huu Anh Quan [a,5]

[a] Faculty of Electrical Engineering, University of Science and Technology, The University of Danang, Da Nang, Vietnam
[1] nkquang@dut.udn.vn; [2] haducphi246@gmail.com; [3] vulephu.010123@gmail.com; [4] tuanphantxqt@gmail.com
[5] grandpinkvip@gmail.com
[*] Corresponding Author

ARTICLE INFO

Article History
Received December 16, 2025
Revised January 30, 2026
Accepted May 05, 2026

SMO;
PMSM;
Chattering Reduction;
FPGA;
FSM

ABSTRACT

This paper presents the design and implementation of a sensorless permanent magnet synchronous motor (PMSM) drive on a field-programmable gate array (FPGA) using a sliding mode observer (SMO) and a phase-locked loop (PLL) for accurate and robust speed/position tracking. To eliminate mechanical position sensors while reducing cost and improving reliability in harsh environments, a chattering-mitigated SMO employing a hyperbolic tangent switching function is developed and integrated with a PLL-based position/speed extraction scheme. Practical FPGA feasibility is emphasized by adopting fixed-point arithmetic and finite-state-machine (FSM) scheduling to achieve deterministic real-time execution and efficient resource sharing, without excessive algorithmic complexity. The proposed scheme is validated through both simulation and real-time experiments on an FPGA platform. Quantitative evaluation under identical conditions shows that, in sensorless operation, the proposed SMO improves tracking accuracy to MAE = 4.5 rpm and RMSE = 6.24 rpm, compared with the sign-based SMO (MAE = 9.4 rpm, RMSE = 13.9 rpm) and the saturation+arctangent SMO (MAE = 7.0 rpm, RMSE = 9.7 rpm), corresponding to reductions of 52.1% (MAE) and 55.1% (RMSE) versus the sign-based baseline. In transient speed reversal, the rising time is reduced from approximately 0.2 s to 0.16 s. Rotor flux-angle estimation error is reduced from about 6°–9° to 2°–4°, with phase delay improved relative to $>$ 25 ms observed in conventional SMO during rapid variations. The FPGA implementation completes each SMO–PLL update in approximately 8.16 μs at 12.5 MHz and utilizes 12,568 LEs, 230,656 RAM bits, and 26 embedded multipliers on MAX10. Importantly, the improved estimation and control performance is achieved with only a modest increase in hardware resources compared with a traditional SMO (an increase of approximately 4% in LEs and approximately 5% in embedded multipliers), reflecting a clear and practical accuracy–resource trade-off. These results demonstrate an efficient, low-cost, and reliable FPGA-based sensorless PMSM drive suitable for industrial servo, robotics, and automation applications with diverse speed profiles and transient disturbances.

1. Introduction

Permanent Magnet Synchronous Motors (PMSMs) have gained significant adoption across industries such as electric vehicles, robotics, aerospace, and precision control systems due to their high efficiency, high power density, simple construction, and wide operating speed range. High-performance strategies such as Field-Oriented Control (FOC) require accurate rotor position and speed information. However, mechanical sensors (e.g., encoders) increase system cost and wiring complexity and may reduce reliability in harsh environments. Consequently, sensorless PMSM control has attracted extensive research attention [1]–[9].

Sensorless control methods can be broadly categorized into two groups: signal-injection approaches, such as high-frequency signal injection (HFSI) methods, and model-based approaches. HFSI methods are suitable for low- and zero-speed operation, but they may introduce acoustic noise and additional losses and often require specialized hardware [1], [2]. Model-based methods are typically effective at medium-to-high speeds and include estimation schemes such as the Model Reference Adaptive System (MRAS), Extended Kalman Filter (EKF), and Sliding Mode Observer (SMO) [9]–[25]. MRAS performance is sensitive to motor parameter variations, often requiring online parameter estimation to maintain accurate position estimation; moreover, parameter adaptation can be challenging and may lead to degraded performance if incorrectly tuned [9]. EKF-based observers provide strong dynamic performance and high estimation accuracy, but they require substantial computation for matrix operations, which is difficult to implement efficiently on fixed-point processors or resource-limited FPGA platforms; tuning the process and measurement noise covariance matrices (Q and R) is also non-trivial, motivating adaptive EKF variants [3]. Reduced-order or parallel EKF architectures have been proposed to lower computational burden and improve feasibility on FPGA, yet the implementation remains relatively complex compared with SMO-based solutions [4].

SMO is widely adopted because of its robustness and comparatively simple structure [4]–[6]. SMO estimates rotor position and speed using back electromotive force (BEMF). However, the conventional SMO commonly employs a discontinuous reaching law (e.g., sign switching), which produces chattering, high-frequency oscillations in the estimated signals. To mitigate chattering, continuous switching functions (e.g., sigmoid, hyperbolic tangent, or piecewise power functions) are often combined with low-pass filters (LPFs) [7]–[11]. Unfortunately, LPF-based smoothing introduces phase delay, creating a trade-off between chattering suppression and estimation accuracy/convergence speed. In addition, computing rotor position directly via the arctangent function from BEMF can be noise-sensitive and may reduce position accuracy, which can limit overall control performance [7], [12]. To improve position/speed extraction from BEMF, PLL-based techniques are frequently used; nevertheless, conventional PLLs may exhibit steady-state lock errors and can lose accuracy during speed reversal. Therefore, various enhanced PLL structures have been reported, including adaptive PLLs, complex bandpass filter (CBF)-assisted PLLs, feed-forward PLLs, and ESO-enhanced PLLs [11], [13]–[15]. In parallel, higher-order and adaptive SMO variants (e.g., super-twisting observers and adaptive fast reaching laws) have been developed to reduce chattering while maintaining robustness and dynamic response, and adaptive laws have been used for online parameter identification and gain tuning to handle parameter variations and noise [7], [11], [14]–[21].

From an implementation standpoint, achieving real-time performance for sensorless PMSM control requires fast and deterministic computation. While DSPs and MCUs are commonly used, FPGAs have become increasingly attractive due to their inherent parallel processing capability, deterministic timing, low control latency, and the possibility of integrating multiple control and estimation modules on a single chip. Several studies have demonstrated FPGA feasibility for sensorless algorithms, including observer-based approaches [3], [4], [21], [22]. However, practical FPGA deployment still faces challenges in fixed-point design, scheduling, and resource efficiency, especially when the control system must remain stable under rapid acceleration/deceleration and transient disturbances [26]–[55].

In this paper, we implement an FPGA-based sensorless PMSM control system that integrates a chattering-mitigated SMO and a PLL for robust rotor position and speed estimation. The SMO employs a hyperbolic tangent switching function to suppress chattering while maintaining robustness, and the PLL improves BEMF-based position/speed extraction and reduces phase-lag effects during rapid transients. To ensure practical FPGA feasibility, we propose an FSM-based scheduling strategy with fixed-point arithmetic for deterministic real-time execution and efficient processing [56-60]. The research contributions are as follows: (i) An FPGA-integrated sensorless PMSM estimation scheme combining a hyperbolic tangent–based chattering-mitigated SMO and PLL for improved rotor position and speed estimation robustness; (ii) An implementation-oriented FSM scheduling design that provides deterministic real-time execution and optimized processing time under fixed-point constraints; and (iii) Comprehensive validation in both simulation and real-time experiments demonstrating improved tracking stability and reduced oscillations/chattering in the estimated signals during speed variations and transients.

The remainder of this paper is organized as follows. Section 2 describes the system and observer design; Section 3 focuses on FPGA design; Section 4 presents the simulation results along with their analysis; Section 5 provides experimental validation; and Section 6 concludes the paper.

2. System Description and Sensorless Speed Control

The sensorless FOC (Field-Oriented Control) speed control structure with the proposed SMO estimation technique is depicted in Fig. 1.

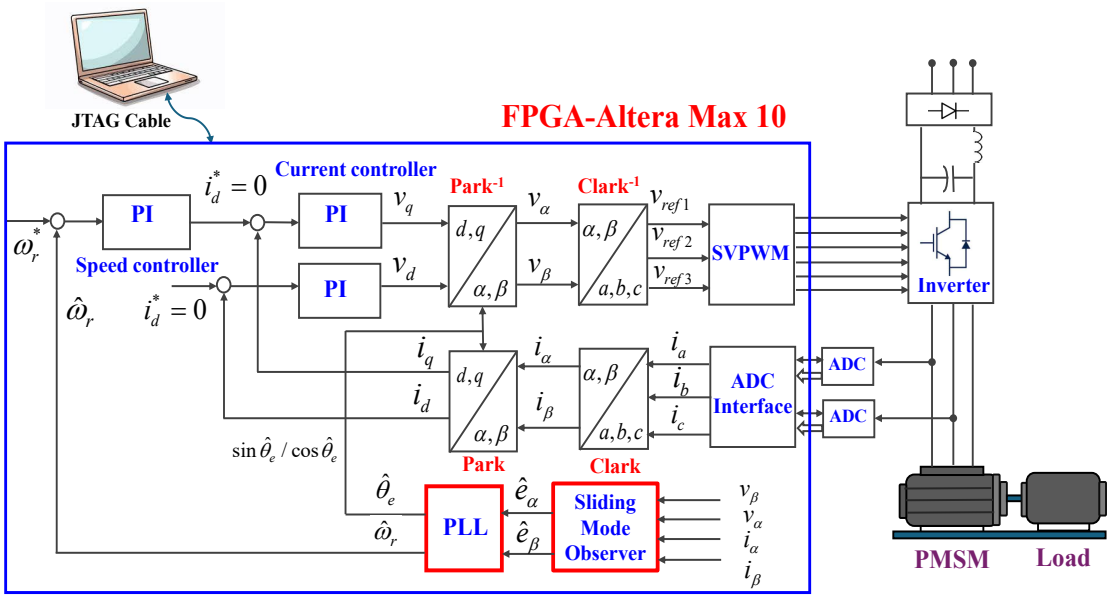

Fig. 1. System architecture for FPGA-based sensorless PMSM drives

2.1. FOC-PMSM Drive Model

The behavior dynamics of the PMSM when subjected to vector control is characterized by a nonlinear and mutually dependent model that is derived from the voltage vector equations:

$$\begin{bmatrix} v_d \\ v_q \end{bmatrix} = \begin{bmatrix} r_s + sL & -\omega_e L \\ \omega_e L & r_s + sL \end{bmatrix} \begin{bmatrix} i_d \\ i_q \end{bmatrix} + \begin{bmatrix} 0 \\ \omega_e \lambda_f \end{bmatrix}, \tag{1}$$

Where r_s denote the stator's winding resistance and the self-inductance along each axis $L_d = L_q \triangleq L$ (IPMSM), while λ_f represents the flux linkage of the permanent magnet, the electrical angular frequency is expressed as ω_e, and P corresponds to the number of rotor pole pairs.

The motor's torque, T_e, generated by the motor of the driving PMSM operating under field-oriented control (with $i_d = 0$) can be expressed as [10]:

$$T_e = \frac{3P}{4}\lambda_f i_q \triangleq K_t i_q, \tag{2}$$

and its dynamic equation is

$$T_e - T_L = J\frac{d}{dt}\omega_r + B\omega_r, \tag{3}$$

Where K_t is torque constant, J is the inertial value, B is damping ratio, T_L is the external torque and ω_r is the speed of the motor.

2.2. Design of Sliding Mode Current Observer

Fig. 2 presents the structure of the newly designed Sliding Mode Observer (SMO), which consists of several key components: a current observer based on sliding mode control theory, a hyperbolic tangent function module, and the phase-locked loop module for estimating rotor speed and position. The system operates with inputs that include the measured stator currents, i_α and i_β, along with the corresponding voltage control signals, v_α and v_β.

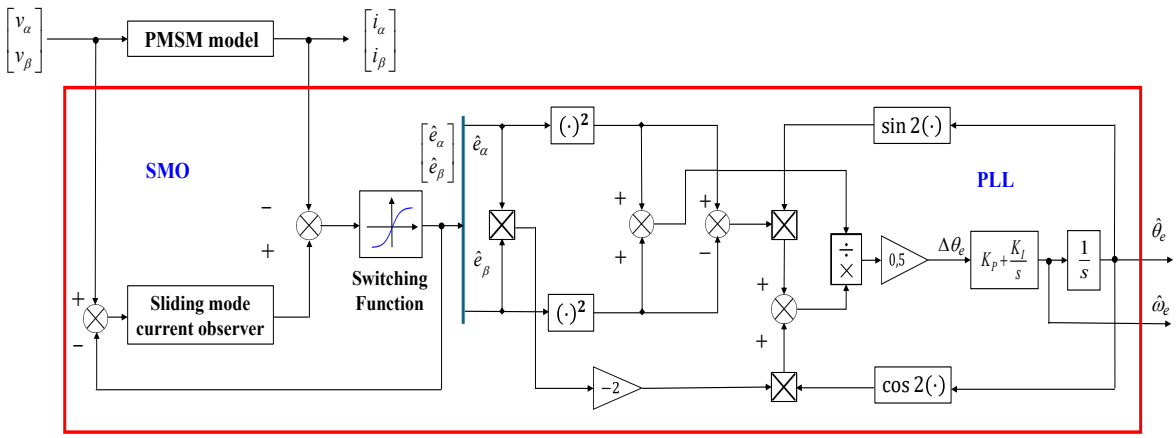

Fig. 2. Rotor position and speed estimation using new SMO

The predicted current values are continuously compared to the actual measured currents, and any resulting discrepancies are processed using the hyperbolic tangent function. This enables the system to estimate the back electromotive force (EMF). Once the back EMF is accurately estimated, the phase-locked loop is used to determine the rotor position and speed. A detailed overview of the SMO mechanism is presented below.

The PMSM model (1) can be rewritten in the stationary $\alpha - \beta$ coordinate frame as,

$$\begin{bmatrix} v_\alpha \\ v_\beta \end{bmatrix} = \begin{bmatrix} r_s + sL & 0 \\ 0 & r_s + sL \end{bmatrix} \begin{bmatrix} i_\alpha \\ i_\beta \end{bmatrix} + \omega_e \lambda_f \begin{bmatrix} -\sin\theta_e \\ \cos\theta_e \end{bmatrix}, \tag{4}$$

Where s denotes the differential operator.

By denoting the back EMF by

$$e = \begin{bmatrix} e_\alpha \\ e_\beta \end{bmatrix} \triangleq \omega_e \lambda_f \begin{bmatrix} -\sin\theta_e \\ \cos\theta_e \end{bmatrix}, \tag{5}$$

we can obtain from (4) the state-space representation for the current variables as,

$$\frac{d}{dt}\begin{bmatrix} i_\alpha \\ i_\beta \end{bmatrix} = -\frac{r_s}{L}\begin{bmatrix} i_\alpha \\ i_\beta \end{bmatrix} + \frac{1}{L}\begin{bmatrix} v_\alpha \\ v_\beta \end{bmatrix} - \frac{1}{L}\begin{bmatrix} e_\alpha \\ e_\beta \end{bmatrix}, \tag{6}$$

An improved sliding mode observer for the currents can be described by:

$$\frac{d}{dt}\begin{bmatrix} \hat{i}_\alpha \\ \hat{i}_\beta \end{bmatrix} = -\frac{r_s}{L}\begin{bmatrix} \hat{i}_\alpha \\ \hat{i}_\beta \end{bmatrix} + \frac{1}{L}\begin{bmatrix} v_\alpha \\ v_\beta \end{bmatrix} - \frac{1}{L}\begin{bmatrix} kF(\hat{i}_\alpha - i_\alpha) \\ kF(\hat{i}_\beta - i_\beta) \end{bmatrix}, \tag{7}$$

Where vector $\begin{bmatrix} \hat{i}_\alpha & \hat{i}_\beta \end{bmatrix}^T$ represents the estimated stator currents in the stationary reference frame, and k denotes the observer gain.

To reduce the chattering effect caused by the discontinuous nature of the sliding mode approach, F is replaced with a smoother, continuous alternative, the hyperbolic tangent function, instead of the conventional signum function, as given by:

$$F(x) = \begin{bmatrix} \dfrac{e^{ax} - e^{-ax}}{e^{ax} + e^{-ax}} \end{bmatrix} = \begin{bmatrix} \dfrac{e^{2ax} - 1}{e^{2ax} + 1} \end{bmatrix}, \tag{8}$$

Where $a > 0$ is a design coefficient. Therefore, by defining the current estimation error of the proposed SMO by

$$\bar{i} = \begin{bmatrix} \bar{i_\alpha} \\ \bar{i_\beta} \end{bmatrix} = \begin{bmatrix} \hat{i}_\alpha - i_\alpha \\ \hat{i}_\beta - i_\beta \end{bmatrix}, \tag{9}$$

and the following observer error system can be obtained:

$$\frac{d}{dt}\begin{bmatrix} \bar{i_\alpha} \\ \bar{i_\beta} \end{bmatrix} = -\frac{r_s}{L}\begin{bmatrix} \bar{i_\alpha} \\ \bar{i_\beta} \end{bmatrix} + \frac{1}{L}\begin{bmatrix} e_\alpha \\ e_\beta \end{bmatrix} - \frac{1}{L}\begin{bmatrix} kF(\bar{i_\alpha}) \\ kF(\bar{i_\beta}) \end{bmatrix}. \tag{10}$$

By choosing an appropriately large observer gain $k > max(|e_\alpha|, |e_\beta|)$ that ensures $\bar{i}^T.\bar{i} < 0$, a sliding mode can be triggered, thereby forcing the current estimation error to converge to zero. After the sliding mode is attained, it follows from the observer error system that the last two terms on the right-hand side of equation (10) must be nullified. As a result, the back EMF components can be estimated as:

$$\begin{bmatrix} e_\alpha \\ e_\beta \end{bmatrix} = k\begin{bmatrix} F(\bar{i_\alpha}) \\ F(\bar{i_\beta}) \end{bmatrix} \triangleq \begin{bmatrix} \hat{e}_\alpha \\ \hat{e}_\beta \end{bmatrix}, \tag{11}$$

Where $\begin{bmatrix} \hat{e}_\alpha & \hat{e}_\beta \end{bmatrix}^T$ is the estimated back EMF vector in the stationary reference frame $(\alpha - \beta)$.

2.3. Speed and Position Estimation

After obtaining the estimated back EMF, the rotor's position can be computed by applying equation (5). This angle is determined using the inverse tangent function as expressed below:

$$\hat{\theta}_e(n) = tan^{-1}\left(\frac{-\hat{e}_\alpha}{\hat{e}_\beta}\right), \tag{12}$$

and the estimated rotor speed can then be approximately determined by

$$\hat{\omega}_e = \frac{d\hat{\theta}_e}{dt}. \tag{13}$$

However, the use of the arctangent function makes the estimation of position and speed more sensitive to noise and harmonic components. In particular, noticeable estimation deviations may occur when $\hat{e}_\beta$ approaches or passes through zero.To mitigate the aforementioned adverse effects, the system employs a phase-locked loop algorithm to stabilize the signal and improve the accuracy of the estimation process. The overall structure of the PLL is illustrated in Fig. 2, and the algorithm will be described in detail in the following.

Considering the deviation between the actual and the estimated rotor positions, the angular error can be defined as,

$$\Delta\theta_e = \theta_e - \hat{\theta}_e. \tag{14}$$

Under the condition $|\theta_e - \hat{\theta}_e| \leq \frac{\pi}{6}$, this error can be approximated by

$$\Delta\theta_e \approx \sin(\theta_e - \hat{\theta}_e) \approx \frac{1}{2}\sin(2\theta_e - 2\hat{\theta}_e). \tag{15}$$

By expanding the trigonometric terms, we obtain

$$\begin{aligned}\Delta\theta_e &= \frac{1}{2}\big[\sin(2\theta_e)\cos(2\hat{\theta}_e) - \cos(2\theta_e)\sin(2\hat{\theta}_e)\big] \\ &= \frac{1}{2}\big[2\sin\theta_e\cos\theta_e\cos(2\hat{\theta}_e) + (\sin^2\theta_e - \cos^2\theta_e)\sin(2\hat{\theta}_e)\big] \\ &= \frac{1}{2E^2}\big[-2e_\alpha e_\beta\cos(2\hat{\theta}_e) + (e_\alpha^2 - e_\beta^2)\sin(2\hat{\theta}_e)\big],\end{aligned} \tag{16}$$

Where $E^2 = e_\alpha^2 + e_\beta^2$.

Based on this angular error, the estimated position can be corrected using a PI controller. The integral action plays a crucial role in eliminating steady-state errors. The control law is expressed as

$$\hat{\theta}_e = \frac{1}{s}\left(K_p + \frac{K_i}{s}\right)\Delta\theta_e. \tag{17}$$

In the Laplace domain, the transfer function of the PLL with a PI controller can be written as

$$G_{\mathrm{PLL}}(s) = \frac{\hat{\theta}_e(s)}{\Delta\theta_e(s)} = \frac{K_p s + K_i}{s^2 + K_p s + K_i}. \tag{18}$$

The controller is designed to achieve fast response and adequate damping. By applying the standard second-order control criterion, the transfer function can be expressed as

$$G_{\mathrm{PLL}}(s) = \frac{\omega_n^2}{s^2 + 2\xi\omega_n s + \omega_n^2}, \tag{19}$$

Where ω_n is the natural frequency and ξ is the damping factor.

By comparing (18) and (19), the controller parameters are determined as $K_p = 2\xi\omega_n$ and $K_i = \omega_n^2$. These parameters are selected to ensure a stable and fast dynamic response while effectively suppressing noise and harmonic disturbances, allowing the rotor angle to be estimated accurately and continuously.

$$\Delta\theta_e(n) \approx \frac{1}{2(e_\alpha^2(n) + e_\beta^2(n))}\left[-2e_\alpha(n)e_\beta(n)\cdot\cos(2\hat{\theta}_e(n)) + (e_\alpha(n)^2 - e_\beta(n)^2)\sin(2\hat{\theta}_e(n))\right] \tag{20}$$

After discretization, the PI controller in the PLL is obtained as follows:

$$u(k) = K_P \Delta\theta_e(n) + u_I(n-1) + K_I \frac{T_s}{2}\big[\Delta\theta_e(n) + \Delta\theta_e(n-1)\big], \tag{21}$$

Where

$$u_I(n) = u_I(n-1) + K_I \frac{T_s}{2}\big[\Delta\theta_e(n) + \Delta\theta_e(n-1)\big] \tag{22}$$

The rotor position is obtained by integrating $u(n)$, expressed as

$$\hat{\theta}_e(n) = \hat{\theta}_e(n-1) + \frac{T_s}{2}\big(u(n) - u(n-1)\big). \tag{23}$$

The estimated electrical speed is derived from the control signal $u(n)$,

$$\hat{\omega}_e(n+1) = \Omega\,\hat{\omega}_e(n) + (1-\Omega)\,u(n), \qquad \Omega = e^{-\omega_c T_s}. \tag{24}$$

The overall procedure for estimating the rotor electrical angle and speed using the proposed SMO–PLL can be summarized as follows.

Step 1: Acquire the measured three-phase currents/voltages and transform them into the stationary frame to obtain $i_\alpha(n)$, $i_\beta(n)$, $v_\alpha(n)$, and $v_\beta(n)$.

Step 2: Update the estimated currents $\hat{i}_\alpha(n)$ and $\hat{i}_\beta(n)$ using the improved SMO dynamics in (7), where the switching function $F(\cdot)$ is implemented by the hyperbolic tangent function in (8).

Step 3: Compute the current estimation errors $i_\alpha(n) = \hat{i}_\alpha(n) - i_\alpha(n)$ and $i_\beta(n) = \hat{i}_\beta(n) - i_\beta(n)$ as defined in (9), then estimate the back-EMF components $\hat{e}_\alpha(n)$ and $\hat{e}_\beta(n)$ using (11).

Step 4: Compute the PLL phase detector output (angular error) $\Delta\theta_e(n)$ based on the back-EMF and the current angle estimate using (20).

Step 5: Update the discrete PI loop filter using (21) and (22), integrate to obtain the refined electrical angle $\hat{\theta}_e(n)$ using (23), and compute the electrical speed $\hat{\omega}_e(n)$ using (24). If the mechanical position is required, it can be obtained as $\hat{\theta}_m(n) = \hat{\theta}_e(n)/P$.

3. FPGA Architecture and FSM Implementation

3.1. FPGA Architecture of Proposed Sensorless Control

The integrated circuit design for sensorless speed control of PMSM motors, utilizing the SMO algorithm and an enhanced PLL, is implemented on an FPGA platform and is shown in Fig. 3. The FPGA chip chosen for this design is the MAX 10 (M50DAF484C7G), manufactured by Altera, offering significant computational resources including 50,000 logic elements, 1,638,000 bits of on-chip RAM, 144 embedded multipliers with 18-bit precision, and up to 672 input/output pins.

The sensorless speed control IP consists of several functionally interconnected modules. Key components include an SMO-based estimation unit integrated with a PLL p to calculate rotor flux angle and angular velocity, a speed PI controller, current regulation modules, and the CCCT block, which synchronizes current control with all reference frame transformations. The system also incorporates Space Vector PWM (SVPWM) modulation and Analog-to-Digital Conversion (ADC) units. To ensure synchronized operation across all components, a frequency divider generates clock signals: 50 MHz (20 ns), 12.5 MHz (80 ns), 5 MHz (200 ns), and 2 MHz (500 ns). Detailed information on the architecture of the CCCT, the current PI controllers, the ADC interface, and the SVPWM design can be found in [3] and [21].

All computational modules operate using a 32-bit fixed-point Q15 format, ensuring precise and consistent numerical processing. The design mainly focuses on the hardware-level implementation

of the sigmoid function, along with the proposed SMO and PLL methods to estimate current and back EMFs in the stationary frame, which subsequently allows the calculation of rotor flux angle and rotational speed. To optimize FPGA logic usage, a Finite State Machine (FSM) is employed to control the execution of these mathematical operations, leveraging an efficient resource-conserving approach. Detailed FSM diagrams are provided in the following sections.

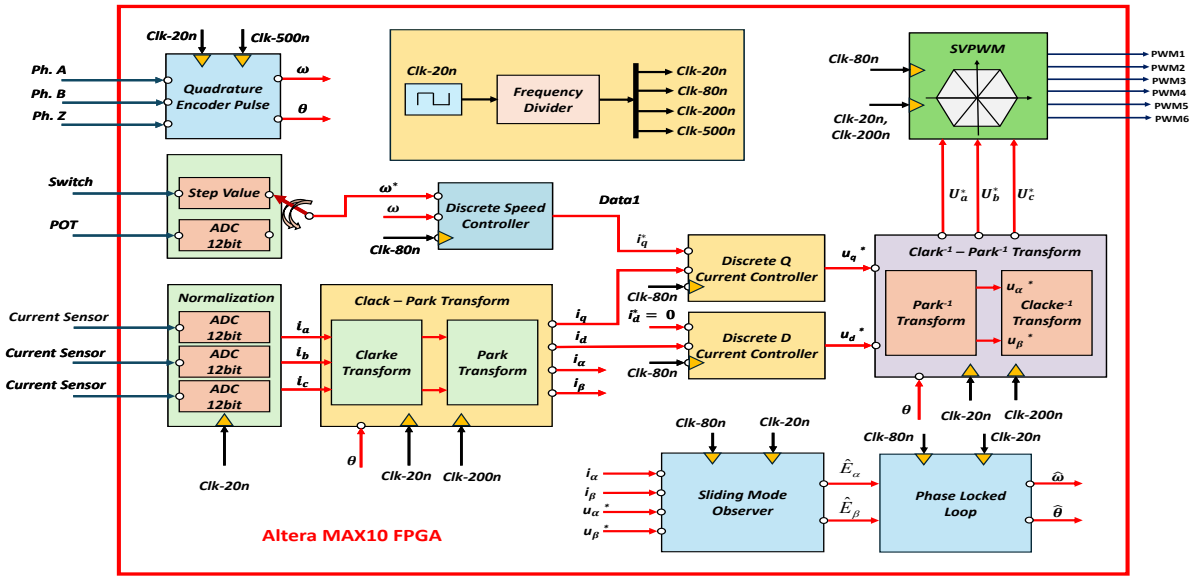

Fig. 3. Proposed IC design for sensorless speed control

3.2. Implementation of SMO with Finite State Machine (FSM)

The circuit architecture of the Sliding Mode Observer combined with Phase-Locked Loop (SMO-PLL), illustrated in Fig. 4, demonstrates an optimal balance between computational accuracy and processing speed. The system consists of one adder, one multiplier, two functional blocks for computing the hyperbolic tangent forcing function, and a PLL block responsible for estimating rotor position and speed, forming a closed-loop processing structure for the entire system.

Numerical computation is performed using a fixed-point system in 32-bit Q15 format, ensuring high efficiency and minimal error. As shown in the figure, the algorithm is organized into a continuous sequence of processing steps: Steps $S_0 - S_7$ execute the sliding-mode current observer; steps $S_8 - S_{28}$ compute the current error, hyperbolic tangent forcing function, and back electromotive force (Back-EMF) along the α-axis, while Steps $S_{29} - S_{48}$ perform similar operations to determine the Back-EMF along the β-axis. Finally, the PLL block estimates the rotor flux position and speed through 52 successive processing steps, as detailed in next section.

With each computational step requiring only 80 ns at a 12.5 MHz clock frequency, the entire SMO-PLL algorithm completes within approximately 8.16 μs, demonstrating fast and stable real-time performance, well-suited for modern permanent-magnet synchronous motor control applications.

3.3. Implementation of Phase-Lock Loop with FSM

Again, by utilizing a fixed-point system with a 32-bit Q15 format and a finite state machine, the algorithm for implementing the PLL function, as shown in the insets of Fig. 4, consists of several adders, multipliers, and a divider. The system processes 52 machine steps to complete the overall computation, as illustrated in Fig. 5. Steps $S_{50} - S_{88}$ compute the angular deviation value using (20); the following steps, from $S_{89} - S_{96}$, perform calculations based on (21) and (23) to estimate the rotor angle; and the final steps, from $S_{97} - S_{102}$, estimate the speed using (24). The entire processing time

for the PLL function is 4.16 µs when operating at a clock frequency of 12.5 MHz.

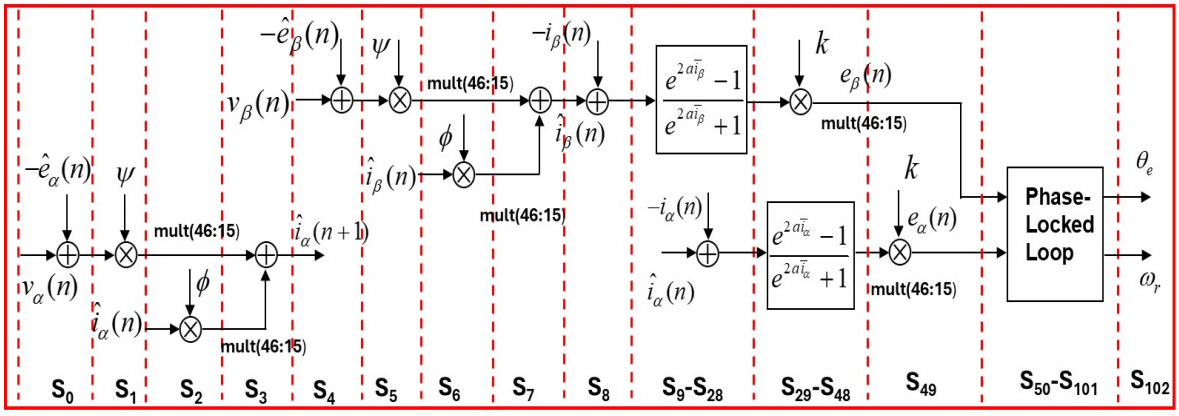

Fig. 4. State machine diagram of the proposed SMO algorithm

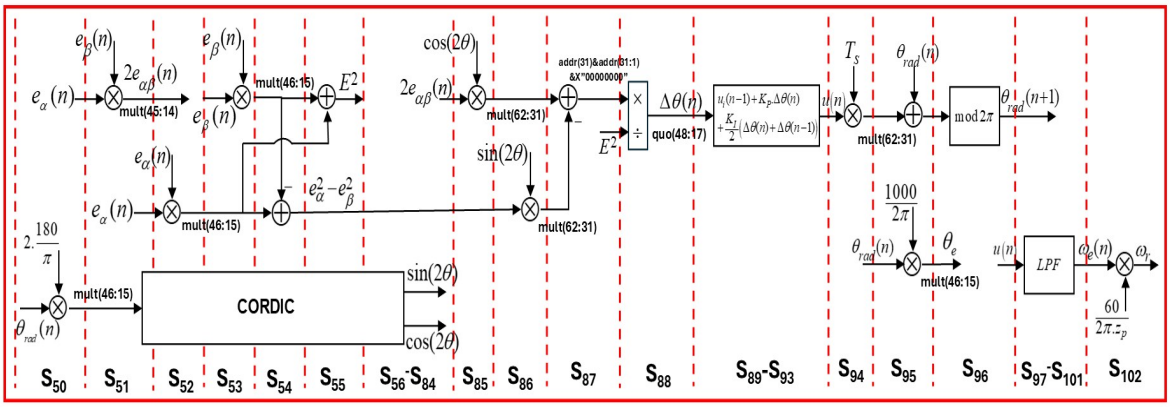

Fig. 5. State machine diagram of PLL algorithm

3.4. Hardware Resource Consumption

The resource utilization of the new sensorless speed control architecture shows that it occupies 12,568 LEs, 230,656 bits of RAM, and 26 embedded 18x18 multipliers, accounting for 24% of the LEs, 2.40% of the RAM, and 18% of the embedded 18x18 multipliers resources of the MAX10 FPGA (model M50DAF484C7G). This is approximately 4% more LEs and 5% more embedded multipliers than the traditional SMO. The difference arises from the addition of the hyperbolic switching function to replace the signum function, as well as the incorporation of a PLL block to compute the rotor angle and speed. Despite these enhancements, the new SMO uses only 24% of the chip's total resources, ensuring the design remains optimized for modern chips with relatively low overall resource consumption.

Most importantly, the new SMO offers significant benefits, including reduced chattering, phase lag, and improved accuracy in estimations and addressing issues that the traditional SMO struggles with. The FSM design technique contributes to considerable chip resource savings by streamlining the logic elements and ensuring efficient utilization. As a result, the proposed approach, with its ability to handle complex conditions while providing superior performance with moderate resource usage, establishes itself as an effective and optimized solution for real-world PMSM control applications using system-on-chip technology.

4. Modelsim/Simulink Co-Simulation and its Results

The Simulink/ModelSim co-simulation architecture for the sensorless PMSM drive is shown in Fig. 6. In this framework, the PMSM and the IGBT inverter are modeled using the SimPowerSystem blockset in Simulink, while the sensorless control and observer algorithms implemented in VHDL are executed cycle-accurately in ModelSim through the EDA co-simulation interface.

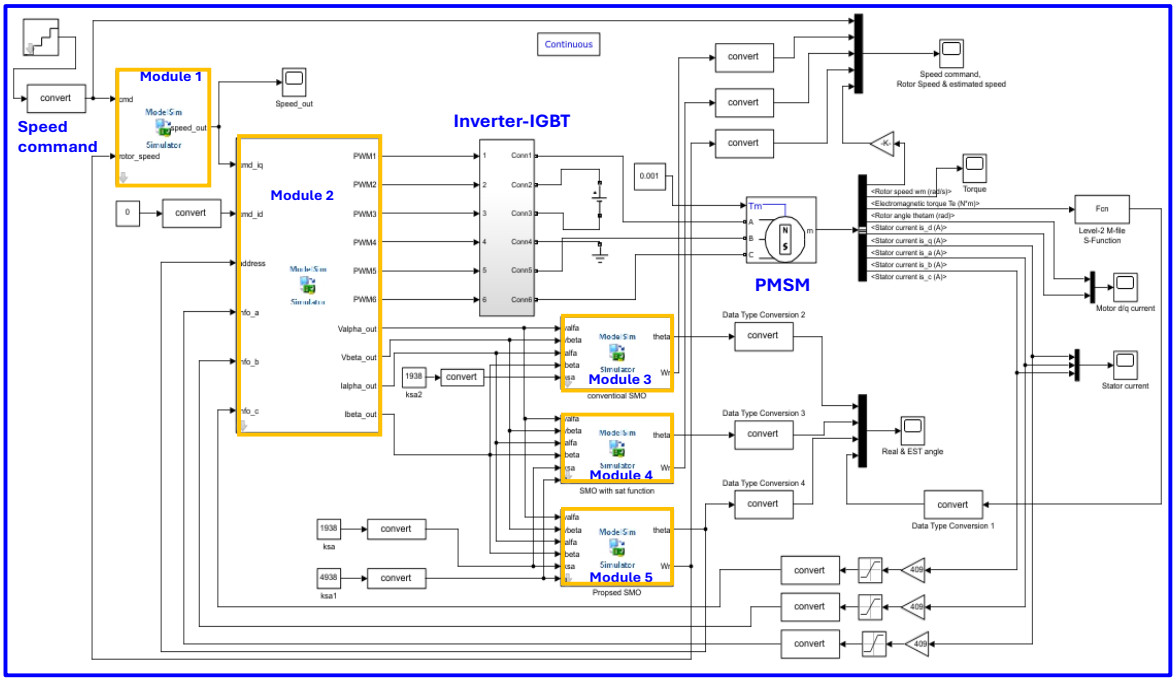

Fig. 6. The simulink/modelsim co-simulation architecture for sensorless speed control system

To ensure a fair and meaningful comparison with prior work, the conventional SMO structures were implemented using the same algorithmic formulation and estimator parameters as reported in previous study [25]. The overall system is divided into five functional modules: (1) the PI speed controller; (2) the current controller with coordinate transformation and SVPWM generation; (3) a conventional SMO using a sign switching function; (4) an SMO with sigmoid switching and arctangent-based angle estimation; and (5) the proposed SMO using a hyperbolic tangent switching function combined with a PLL. The current loop and SMO update run at 16 kHz, whereas the speed loop operates at 2 kHz, with synchronized 50 MHz and 12.5 MHz clock sources supplying the ModelSim execution.

The simulated motor is an eight-pole PMSM ($2P = 8$) with parameters $r_s = 4.75\ \Omega$, $L = 6.55\ \text{mH}$, $J = 1.25 \times 10^{-4}\ \text{kgm}^2$, and $B = 4.47 \times 10^{-6}\ \text{Nms/rad}$. All three observers use identical design parameters ($k = 65$, $a = 0.55$) to ensure a fair comparison. The test scenario consists of forward operation at $500\ \text{rpm}$ under a $0.48\ \text{Nm}$ load, followed by an abrupt reversal to $-500\ \text{rpm}$ at $t = 1\ \text{s}$. The resulting speed and rotor–flux–angle waveforms are shown in Fig. 7(a) and Fig. 7(b), respectively. To quantitatively assess performance, tracking-error metrics were computed under identical conditions. The sensored benchmark achieves $\text{MAE} = 3.05\ \text{rpm}$ and $\text{RMSE} = 7.21\ \text{rpm}$. In contrast, the sign-based SMO yields the largest errors ($\text{MAE} = 9.4\ \text{rpm}$, $\text{RMSE} = 13.9\ \text{rpm}$), followed by the sigmoid+arctangent estimator ($\text{MAE} = 7.0\ \text{rpm}$, $\text{RMSE} = 9.7\ \text{rpm}$). The proposed tanh-based SMO–PLL significantly improves performance, achieving $\text{MAE} = 4.5\ \text{rpm}$ and $\text{RMSE} = 6.24\ \text{rpm}$ closely approaching the sensored baseline.

Fig. 7(a) further shows that although all observers follow the reference speed without overshoot,

the traditional SMOs suffer from noticeably slower dynamics and visible chattering. The sign-based SMO exhibits a rising time of approximately 0.2 s, while the proposed method reaches the target in about 0.16 s. This faster convergence is clearly seen in the zoomed-in regions of Fig. 7(a). The corresponding rotor flux angle results in Fig. 7(b) reinforce these observations. The sign-based and sigmoid-based SMOs show flux-angle errors of $6°$–$9°$ and a phase delay exceeding 25 ms during rapid angle transitions, together with strong oscillations in the estimated signals. In contrast, the proposed SMO–PLL reduces the angle error to $2°$–$4°$, substantially suppresses oscillations, and delivers a much smoother and more stable estimation trajectory. The improvement is especially evident in the magnified views of Fig. 7(b).

Overall, the co-simulation results demonstrate that the hyperbolic-tangent SMO combined with a PLL offers clear advantages over conventional SMOs, including markedly reduced chattering, lower angle error, shorter rising time, and improved robustness during rapid dynamic changes. These results confirm the enhanced precision and stability of the proposed observer, supporting its suitability for practical sensorless PMSM drive applications.

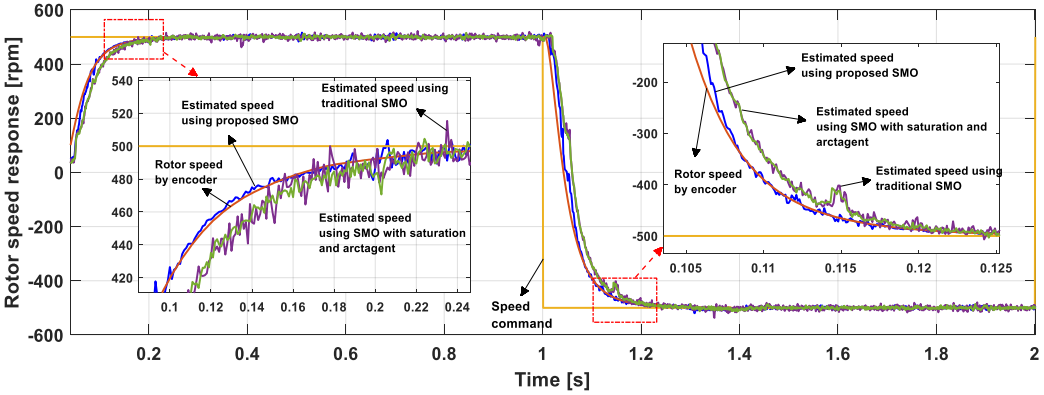

(a) Speed response

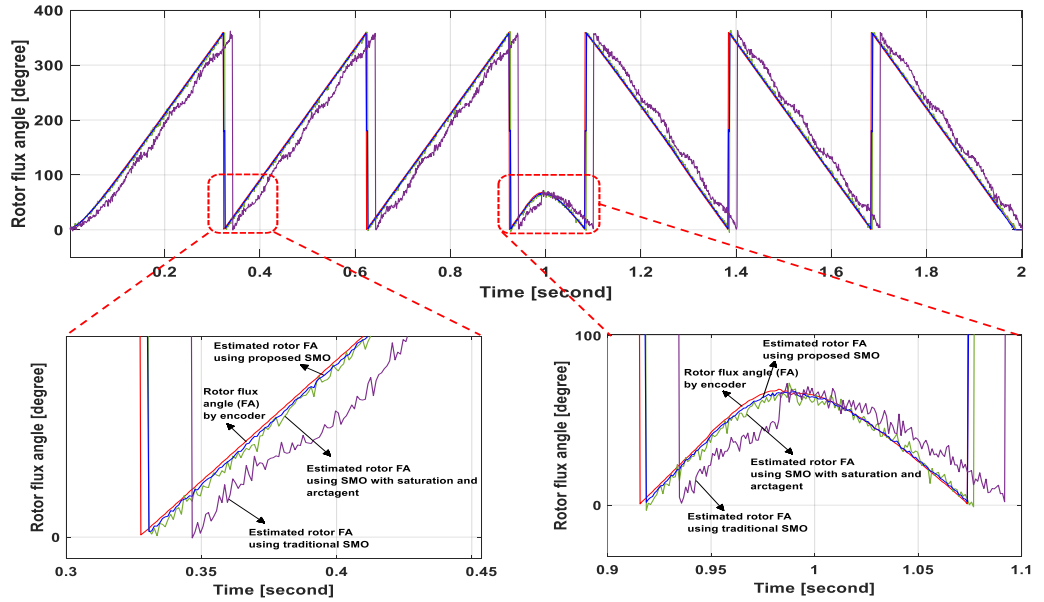

(b) rotor position response

Fig. 7. Rotor speed and flux angle estimation performance between the conventional and proposed SMOs

5. Experimental Validation

After being successfully validated through simulation, the proposed sensorless control method incorporating the new SMO observer was directly implemented on an FPGA platform for a real PMSM drive system to assess its operational performance. The hardware configuration of the sensorless PMSM control setup, consisting of an embedded control module and an IGBT-based inverter, is illustrated in Fig. 8. The PMSM employed in the experiment is rated at 100 W, 100 V, and 1.7 A, operating at 3000 rpm with a torque of 0.32 Nm. An optical encoder with a resolution of 1000 pulses/rev is attached to the motor shaft to provide reference position feedback. The drive utilizes a 6-IGBT inverter bridge capable of handling up to 500 V and 20 A, driven by PWM signals generated from the FPGA.

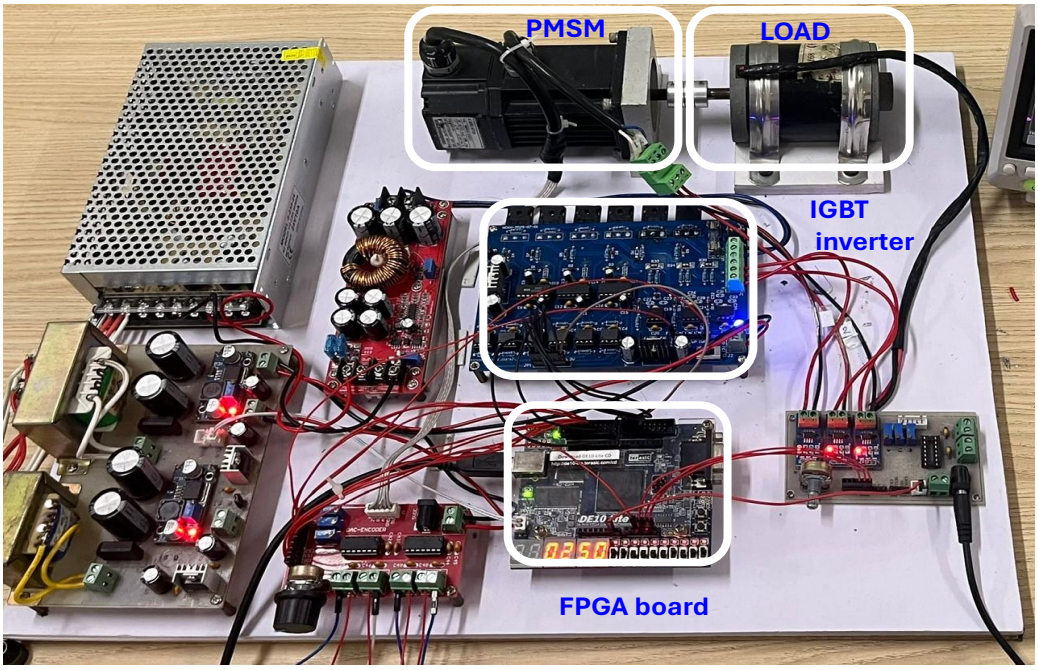

Fig. 8. Setup photograph

The embedded control system is implemented on an Intel MAX10 FPGA, featuring 50,000 logic elements and 1,638,000 bits of on-chip RAM. The SMO algorithm is fully programmed in VHDL, with the design parameters $k = 65$ and $a = 0.55$, identical to those used in the co-simulation stage. The experimental verification scenario mirrors the simulation setup, ensuring consistency in parameter application throughout the testing process.

The experimental results presented in Fig. 9(a) and Fig. 9(b) demonstrate that the proposed observer achieves accurate estimation of both rotor flux angle and motor speed during forward and reverse operation at speeds of 500 rpm and -500 rpm respectively. These findings align closely with the co-simulation outcomes and confirm the robustness and high performance of the FPGA-based sensorless control architecture using the SMO for PMSM drive applications under varying dynamic conditions.

In addition, Fig. 10 shows the rotor-speed estimation under three successive low-speed commands of 100 rpm, 200 rpm, and 300 rpm, followed by a step-load disturbance of 0.48 Nm applied at the steady-state operating point of 200 rpm. At the initial 100 rpm condition (approximately 5% of rated speed), where the back-EMF magnitude is weak, the proposed tanh-SMO–PLL remains stable, providing continuous speed tracking without loss of observability. Minor estimation ripple is visible,

but no divergence or instability is observed, confirming that the proposed observer performs reliably at low speeds. During the subsequent speed transitions from 100 rpm to 200 rpm and from 200 rpm to 300 rpm, the estimated speed follows the reference with smooth transient behavior and limited overshoot. Compared to conventional SMO structures, oscillatory components are significantly reduced, and the response exhibits well-damped convergence after each step command.

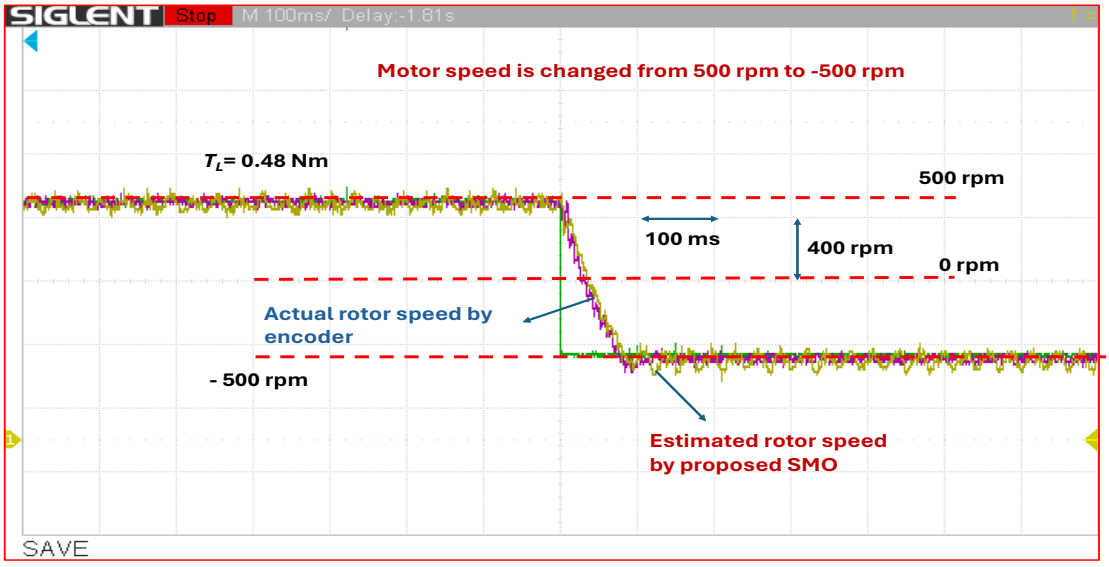

(a) Speed step response

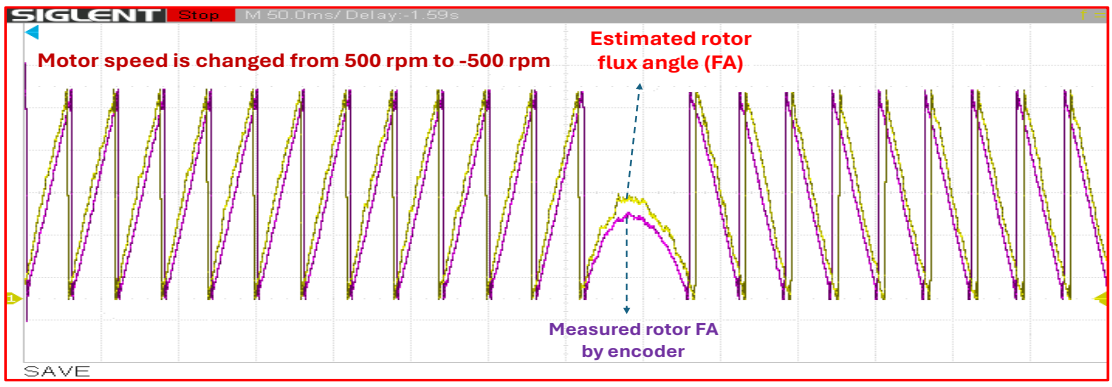

(b) Estimated and measured flux angles during speed changes

Fig. 9. Experimental speed step response from 500 rpm to –500 rpm and the corresponding flux angle

To further evaluate robustness against external disturbances, a step-load torque of 0.48 Nm is applied at 200 rpm. The estimated speed experiences a brief deviation immediately after the load application, followed by rapid recovery to the reference value. The settling process is monotonic and free of sustained oscillations, indicating effective disturbance rejection. This demonstrates that the combined tanh-based SMO and PLL can preserve estimation stability and control performance even under abrupt mechanical loading.

These experimental results confirm that the proposed SMO–PLL architecture not only improves transient smoothness at medium speeds but also maintains stable sensorless operation at low speeds (down to 100 rpm) and during step-load disturbances. The low-speed performance indicates the system's ability to effectively track rotor speed under weak back-EMF conditions, while the fast recovery

from load disturbances ensures minimal impact on system stability. From a practical perspective, the reduced speed ripple and fast recovery directly translate into lower torque pulsation and improved current regulation in the FOC loop, which are essential for servo and robotic applications involving frequent speed changes and load variations. Nevertheless, as with other back-EMF–based sensorless methods, estimation accuracy is expected to degrade further toward zero speed due to diminishing EMF amplitude. Future work will therefore focus on hybrid integration with signal-injection techniques to enhance observability in the near-zero-speed region.

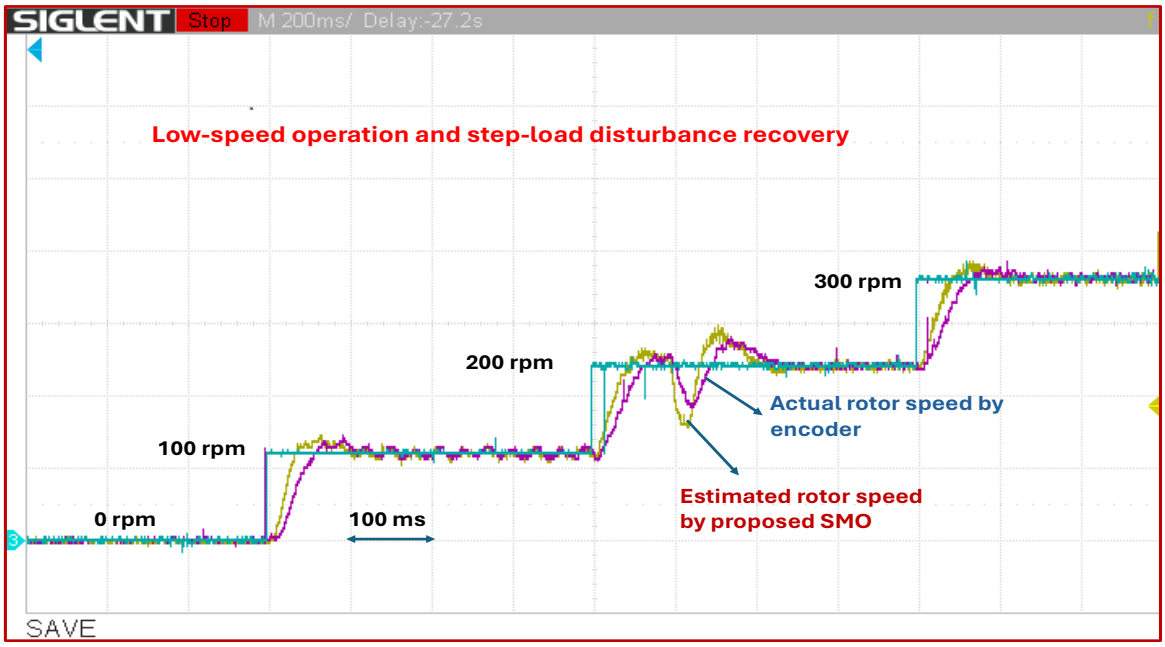

Fig. 10. Low speed operation and step-load disturbance recovery

6. Conclusion

This paper presented the design, FPGA implementation, and experimental validation of a sensorless PMSM drive based on a chattering-mitigated Sliding Mode Observer combined with a Phase-Locked Loop. By replacing the discontinuous sign switching function with a smooth hyperbolic tangent function and integrating PLL-based rotor position and speed estimation, the proposed observer improves estimation accuracy, suppresses chattering, and enhances stability under both steady-state and transient operating conditions. The complete control architecture was implemented on an Altera MAX10 FPGA using 32-bit fixed-point arithmetic and an FSM-based scheduling strategy, ensuring deterministic real-time execution with efficient utilization of hardware resources.

Co-simulation and experimental results demonstrate that the proposed SMO–PLL structure provides fast transient response, accurate speed tracking, and robust estimation performance over a wide operating range. Compared with conventional SMO implementations, the proposed approach achieves shorter rising time, smaller rotor flux-angle error, and significantly smoother estimated signals, while maintaining real-time feasibility on FPGA with only modest resource overhead. These results confirm the practical suitability of the proposed observer for embedded sensorless PMSM drives in industrial servo and automation applications. Future work will focus on extending the applicability of the proposed method toward extreme operating conditions, such as near-zero-speed operation, and on investigating adaptive or hybrid estimation strategies to further enhance robustness under parameter variations and complex disturbance profiles.

Author Contribution: Nguyen Khanh Quang: Writing - original draft, Validation, Supervision, Methodology, Investigation, Hardware, Software, Funding acquisition, Formal analysis;
Ha Duc Phi: Writing - original draft, Hardware, Software, Methodology, Project administration;
Lê Phu Vu: Project administration, Hardware, Software, Conceptualization;
Phan Minh Tuan: Hardware, Software, Conceptualization;
Nguyen Huu Anh Quan: Visualization, Software, Conceptualization.

Funding: This research received no external funding.

Acknowledgment: This work was supported by The University of Danang, University of Science and Technology, code number of Project: T2025-02-04.

Conflicts of Interest: The authors declare no conflict of interest.

References

[1] H. Li, X. Zhang, C. Xu and J. Hong, "Sensorless Control of IPMSM Using Moving-Average-Filter Based PLL on HF Pulsating Signal Injection Method," in *IEEE Transactions on Energy Conversion*, vol. 35, no. 1, pp. 43-52, 2020, https://doi.org/10.1109/TEC.2019.2946888.

[2] S. I. Kim, J. H. Im, E. Y. Song and R. -Y. Kim, "A New Rotor Position Estimation Method of IPMSM Using All-Pass Filter on High-Frequency Rotating Voltage Signal Injection," *IEEE Transactions on Industrial Electronics*, vol. 63, no. 10, pp. 6499-6509, 2016, http://dx.doi.org/10.1109/TIE.2016.2592464.

[3] Y. S. Kung, N. K. Quang and L. T. Van Anh, "FPGA-based neural fuzzy controller design for PMLSM drive," *2009 International Conference on Power Electronics and Drive Systems*, pp. 222-227, 2009, https://doi.org/10.1109/PEDS.2009.5385809.

[4] N. K. Quang, N. T. Hieu and Q. P. Ha, "FPGA-Based Sensorless PMSM Speed Control Using Reduced-Order Extended Kalman Filters," in *IEEE Transactions on Industrial Electronics*, vol. 61, no. 12, pp. 6574-6582, 2024, https://doi.org/10.1109/TIE.2014.2320215.

[5] J. B. Park and X. Wang, "Sensorless direct torque control of surface-mounted permanent magnet synchronous motors with nonlinear Kalman filtering," *Energies*, vol. 11, no. 4, p. 969, 2018, https://doi.org/10.3390/en11040969.

[6] S. Lin and W. Zhang, "An adaptive sliding-mode observer with a tangent function-based PLL structure for position sensorless PMSM drives," *International Journal of Electrical Power & Energy Systems*, vol. 88, pp. 63–74, 2017, https://doi.org/10.1016/j.ijepes.2016.12.006.

[7] S. Chen, X. Zhang, X. Wu, G. Tan, and X. Chen, "Sensorless control for IPMSM based on adaptive super-twisting sliding-mode observer and improved phase-locked loop," *Energies*, vol. 12, no. 7, p. 1225, 2019, https://doi.org/10.3390/en12071225.

[8] K. Kyslan *et al*., "A comparative study and optimization of switching functions for sliding-mode observer in sensorless control of PMSM," *Energies*, vol. 15, no. 7, p. 2689, 2022, https://doi.org/10.3390/en15072689.

[9] L. Yuan, K. Han, C. Zhang, X. Zhu and Y. Ding, "Comparative Analysis of Full-Order SMO and STM-MRAS in SPMSM Sensorless Drive System," in *IEEE Journal of Emerging and Selected Topics in Power Electronics*, vol. 12, no. 3, pp. 2592-2603, 2024, https://doi.org/10.1109/JESTPE.2024.3378806.

[10] Y. Zuo, C. Lai and K. L. V. Iyer, "A Review of Sliding Mode Observer Based Sensorless Control Methods for PMSM Drive," in *IEEE Transactions on Power Electronics*, vol. 38, no. 9, pp. 11352-11367, 2023, https://doi.org/10.1109/TPEL.2023.3287828.

[11] Z. Yin, Y. Zhang, X. Cao, D. Yuan and J. Liu, "Estimated Position Error Suppression Using Novel PLL for IPMSM Sensorless Drives Based on Full-Order SMO," in *IEEE Transactions on Power Electronics*, vol. 37, no. 4, pp. 4463-4474, 2022, https://doi.org/10.1109/TPEL.2021.3125024.

[12] A. A. Dawara, Z. Chen, X. Zhang, H. Zhang, G. Luo and R. Kennel, "An Improved Type-2 Phase-Locked Loop-Based Sliding Mode Observer for Sensorless Control of SPMSM," *2021 IEEE 4th Student Conference on Electric Machines and Systems*, pp. 1-6, 2021, https://doi.org/10.1109/SCEMS52239.2021.9646128.

[13] H. Ding, X. Zou and J. Li, "Sensorless Control Strategy of Permanent Magnet Synchronous Motor Based on Fuzzy Sliding Mode Observer," in *IEEE Access*, vol. 10, pp. 36743-36752, 2022, https://doi.org/10.1109/ACCESS.2022.3164519.

[14] G. Liu, H. Zhang and X. Song, "Position-Estimation Deviation-Suppression Technology of PMSM Combining Phase Self-Compensation SMO and Feed-Forward PLL," in *IEEE Journal of Emerging and Selected Topics in Power Electronics*, vol. 9, no. 1, pp. 335-344, 2021, https://doi.org/10.1109/JESTPE.2020.2967508.

[15] D. Wang, B. Li and Y. Zhao, "An Adaptive SMO Approach for Low-Chattering Sensorless Control of PMSM," in *IEEE Transactions on Power Electronics*, vol. 40, no. 10, pp. 15329-15338, 2025, https://doi.org/10.1109/TPEL.2025.3535457.

[16] H. Sun, X. Zhang, X. Liu and H. Su, "Adaptive Robust Sensorless Control for PMSM Based on Improved Back EMF Observer and Extended State Observer," in *IEEE Transactions on Industrial Electronics*, vol. 71, no. 12, pp. 16635-16643, 2024, https://doi.org/10.1109/TIE.2024.3398688.

[17] D. Jin, L. Liu, Q. Lin and D. Liang, "Sensorless Control Strategy of PMSM With Disturbance Rejection Based on Adaptive Sliding Mode Control Law," in *IEEE Transactions on Transportation Electrification*, vol. 10, no. 3, pp. 5424-5438, 2024, https://doi.org/10.1109/TTE.2023.3327144.

[18] M. Gu *et al*., "Sensorless FCS-MPCC PMSM Drives With Improved Sliding Mode Observer and Low-Complexity Discrete Vector Selection – An Assessment," in *IEEE Transactions on Energy Conversion*, vol. 40, no. 1, pp. 208-217, 2025, https://doi.org/10.1109/TEC.2024.3427703.

[19] X. Xiao, Y. Zhang, J. Wang, and H. Du, "New adaptive sliding-mode observer design for sensorless control of PMSM in electric vehicle drive system," *International Journal on Smart Sensing and Intelligent Systems*, vol. 9, no. 1, pp. 377–396, 2023, https://doi.org/10.21307/ijssis-2017-875.

[20] W. Bai, J. Cai, Y. Kuang, Y. Wang, X. Hua, and Z. Ma, "Research on a novel adaptive sliding mode observer sensorless control for dual three-phase permanent magnet synchronous motors," *Results in Engineering*, vol. 27, p. 105709, 2025, https://doi.org/10.1016/j.rineng.2025.105709.

[21] v. -Q. -B. Ngo, N. Kim Anh and N. Khanh Quang, "FPGA-Based Adaptive PID Controller Using MLP Neural Network for Tracking Motion Systems," in *IEEE Access*, vol. 12, pp. 91568-91574, 2024, https://doi.org/10.1109/ACCESS.2024.3422015.

[22] Z. Ma and X. Zhang, "FPGA Implementation of Sensorless Sliding Mode Observer With a Novel Rotation Direction Detection for PMSM Drives," in *IEEE Access*, vol. 6, pp. 55528-55536, 2018, https://doi.org/10.1109/ACCESS.2018.2871730.

[23] S. Carbone, V. D. Colli, R. Di Stefano, G. Figalli and F. Marignetti, "Design and implementation of high performance FPGA control for permanent magnet synchronous motor," *2009 35th Annual Conference of IEEE Industrial Electronics*, pp. 2901-2906, 2009, https://doi.org/10.1109/IECON.2009.5415265.

[24] G. Yao, J. Zhou, Y. Xiao, D. Jia, and Z. Wang, "Study on the sensorless control method of permanent magnet synchronous motor based on self-tuned boundary layer and RBF neural network," *Results in Engineering*, vol. 27, p. 105816, 2025, https://doi.org/10.1016/j.rineng.2025.105816.

[25] C. Zhang, X. Tang, K. Xing and H. Zhou, "Sensorless Control of Permanent Magnet Synchronous Motors Based on Novel Position Angle Extraction With SMO," in *IEEE Access*, vol. 12, pp. 107008-107016, 2024, https://doi.org/10.1109/ACCESS.2024.3437428.

[26] G. Liu, H. Zhang and X. Song, "Position-Estimation Deviation-Suppression Technology of PMSM Combining Phase Self-Compensation SMO and Feed-Forward PLL," in *IEEE Journal of Emerging and Selected Topics in Power Electronics*, vol. 9, no. 1, pp. 335-344, 2021, https://doi.org/10.1109/JESTPE.2020.2967508.

[27] J. Hu, Z. Wang, H. Wang and C. He, "Gain Compensation-Based Quasi-Resonant PLL With Adaptive Super-Twisting SMO for Position Error Suppression of IPMSM Sensorless Control," in *IEEE Journal of Emerging and Selected Topics in Power Electronics*, vol. 12, no. 5, pp. 4888-4899, 2024, https://doi.org/10.1109/JESTPE.2024.3446643.

[28] H. Cheng, S. Sun, X. Zhou, D. Shao, S. Mi and Y. Hu, "Sensorless DPCC of PMLSM Using SOGI-PLL-Based High-Order SMO With Cogging Force Feedforward Compensation," in *IEEE Transactions on Transportation Electrification*, vol. 8, no. 1, pp. 1094-1104, 2022, https://doi.org/10.1109/TTE.2021.3109018.

[29] Z. Yin, Y. Zhang, X. Cao, D. Yuan and J. Liu, "Estimated Position Error Suppression Using Novel PLL for IPMSM Sensorless Drives Based on Full-Order SMO," in *IEEE Transactions on Power Electronics*, vol. 37, no. 4, pp. 4463-4474, 2022, https://doi.org/10.1109/TPEL.2021.3125024.

[30] D. Wang, B. Li and Y. Zhao, "An Adaptive SMO Approach for Low-Chattering Sensorless Control of PMSM," in *IEEE Transactions on Power Electronics*, vol. 40, no. 10, pp. 15329-15338, 2025, https://doi.org/10.1109/TPEL.2025.3535457.

[31] S. R and B. Singh, "Sensorless Predictive Control of SPMSM-Driven Light EV Drive Using Modified Speed Adaptive Super Twisting Sliding Mode Observer With MAF-PLL," in *IEEE Journal of Emerging and Selected Topics in Industrial Electronics*, vol. 2, no. 1, pp. 42-52, 2021, https://doi.org/10.1109/JESTIE.2020.3014866.

[32] B. Bekhiti, G. Fragulis, K. Hariche, and A. Sharkawy, "Artificial intelligence-enhanced sensorless vector control of induction motors using adaptive neuro-fuzzy systems: Experimental validation and benchmark analysis," *International Journal of Robotics and Control Systems*, vol. 5, no. 3, pp. 1828–1849, 2025, http://dx.doi.org/10.31763/ijrcs.v5i3.1950.

[33] L. Guo, W. Xu, N. Jin and H. Xiao, "A DC-Offset Removed Sensorless Control Method for PMSM Based on SMO With an Improved Prefilter and a Speed Immune Position Error Compensation Strategy," in *IEEE Transactions on Power Electronics*, vol. 40, no. 4, pp. 5163-5176, 2025, https://doi.org/10.1109/TPEL.2024.3524749.

[34] H. Ding, X. Zou and J. Li, "Sensorless Control Strategy of Permanent Magnet Synchronous Motor Based on Fuzzy Sliding Mode Observer," in *IEEE Access*, vol. 10, pp. 36743-36752, 2022, https://doi.org/10.1109/ACCESS.2022.3164519.

[35] J. -P. Chang and M. -Y. Cheng, "Rotor Position Estimation for a Position-Sensorless FOC PMSM Drive—A Super-Twisting-Based Sliding Mode Observer Approach," in *IEEE Access*, vol. 13, pp. 164540-164551, 2025, https://doi.org/10.1109/ACCESS.2025.3611005.

[36] M. Elnaggar, F. Aymen, and D. Mourad, "Sensorless speed estimation basing on MRAS model for a PMSM machine application," *International Journal of Robotics & Control Systems*, vol. 4, no. 4, p. 1694, 2024, https://doi.org/10.31763/ijrcs.v4i4.1585.

[37] H. Yang, A. Xu, Y. Zhang and X. Chai, "Error Analysis and Design of Sliding-Mode-Observer-Based Sensorless PMSM Drives Under a Low Sampling Ratio," in *IEEE Transactions on Power Electronics*, vol. 39, no. 7, pp. 7783-7792, 2024, https://doi.org/10.1109/TPEL.2024.3386820.

[38] Y. Zhong, H. Lin, J. Wang and H. Yang, "Improved Adaptive Sliding-Mode Observer Based Position Sensorless Control for Variable Flux Memory Machines," in *IEEE Transactions on Power Electronics*, vol. 38, no. 5, pp. 6395-6406, 2023, https://doi.org/10.1109/TPEL.2023.3235594.

[39] L. Tao, J. Wang and L. Zhou, "Position Error Correction for Sensorless Control of PMSM Based on Robust Extended State Observer With Inductance Estimation," in *IEEE Transactions on Transportation Electrification*, vol. 11, no. 2, pp. 6132-6142, 2025, https://doi.org/10.1109/TTE.2024.3498857.

[40] M. Sawy, O. Kamel, Y. Mohamed, and M. Mossa, "Dynamic performance evaluation of a brushless AC motor drive using different sensorless schemes," *International Journal of Robotics & Control Systems,*, vol. 4, no. 2, p. 502, 2024, https://doi.org/10.31763/ijrcs.v4i2.1306.

[41] L. Guo, Q. Ye, N. Jin, Z. Liu and Z. Wu, "Sliding-Mode Observer-Based Grid Voltage-Observation Method with Frequency-Fixed Dual SOGI and Cross-Compensated Phase-Locked Loop," in *Chinese Journal of Electrical Engineering*, vol. 10, no. 3, pp. 37-49, 2024, https://doi.org/10.23919/CJEE.2024.000090.

[42] N. Khanh Quang, V. -Q. -B. Ngo, N. Kim Anh, H. Than, T. That Dong and N. Duc Tho, "Neural Network PID Controller for PMSM Drives," *2022 7th National Scientific Conference on Applying New Technology in Green Buildings (ATiGB)*, pp. 146-149, 2022, https://doi.org/10.1109/ATiGB56486.2022.9984109.

[43] W. Xu, S. Qu, and H. Zhang, "A composite sliding-mode observer with PLL structure for a sensorless SPMSM system," *International Journal of Electrical Power & Energy Systems*, vol. 143, p. 108510, 2022, 7https://doi.org/10.1016/j.ijepes.2022.108510.

[44] C. E. Castañeda, A. V. -Gonzalez, H. A. Gabbar, and V. K. Sood, "High-precision speed control of induction motors using a multi-pulse voltage source converter and advanced observer-based strategies," *e-Prime - Advances in Electrical Engineering, Electronics and Energy*, vol. 11, p. 100884, 2025, https://doi.org/10.1016/j.prime.2024.100884.

[45] G. Wang and H. Zhang, "A new speed adaptive estimation method based on an improved flux sliding-mode observer for the sensorless control of PMSM drives," *ISA Transactions*, vol. 128, pp. 675–685, 2022, https://doi.org/10.1016/j.isatra.2021.09.003.

[46] G. Yao, Z. Yang, S. Han, and Z. Wang, "Full-speed domain position sensorless control strategy for PMSM based on a novel phase-locked loop," *Control Engineering Practice*, vol. 152, p. 106058, 2024, https://doi.org/10.1016/j.conengprac.2024.106058.

[47] W. Li, J. Jiang, and J. Mu, "Feedforward-loop phase-locked loop based estimation scheme for sensorless IPMSM drive system," *e-Prime - Advances in Electrical Engineering, Electronics and Energy*, vol. 4, p. 100116, 2023, https://doi.org/10.1016/j.prime.2023.100116.

[48] H. Bai, B. Yu, and W. Gu, "Research on position sensorless control of RDT motor based on improved SMO with continuous hyperbolic tangent function and improved feedforward PLL," *Journal of Marine Science and Engineering*, vol. 11, no. 3, p. 642, 2023, https://doi.org/10.3390/jmse11030642.

[49] T. Sapmaz and A. F. Bakan, "Experimental evaluation of pulsating and rotating HFI methods with adaptive-gain SMO for sensorless IPM compressor drives," *World Electric Vehicle Journal*, vol. 16, no. 12, p. 669, 2025, https://doi.org/10.3390/wevj16120669.

[50] G. Yao, X. Wang, Z. Wang, and Y. Xiao, "Senseless control of permanent magnet synchronous motors based on new fuzzy adaptive sliding mode observer," *Electronics*, vol. 12, no. 15, p. 3266, 2023, https://doi.org/10.3390/electronics12153266.

[51] Z. Li, Z. Zhang, J. Wang, S. Wang, X. Chen, and H. Sun, "ADRC control system of PMLSM based on novel non-singular terminal sliding mode observer," *Energies*, vol. 15, no. 10, p. 3720, 2022, https://doi.org/10.3390/en15103720.

[52] Y. Li, H. Hu, and P. Shi, "A review of position sensorless compound control for PMSM drives," *World Electric Vehicle Journal*, vol. 14, no. 2, p. 34, 2023, https://doi.org/10.3390/wevj14020034.

[53] W. Yang, H. Guo, X. Sun, Y. Wang, S. Riaz, and H. Zaman, "Wide-speed-range sensorless control of IPMSM," *Electronics*, vol. 11, no. 22, p. 3747, 2022, https://doi.org/10.3390/electronics11223747.

[54] Y. Xu, M. Yao, and X. Sun, "Overview of position-sensorless technology for permanent magnet synchronous motor systems," *World Electric Vehicle Journal*, vol. 14, no. 8, p. 212, 2023, https://doi.org/10.3390/wevj14080212.

[55] J. Liang, J. Wu, Y. Wang, Z. Zhong, and X. Bai, "Sensorless control for a permanent magnet synchronous motor based on a sliding mode observer," *Eng*, vol. 5, no. 3, pp. 1737–1751, 2024, https://doi.org/10.3390/eng5030091.

[56] C. He, S. Xu, B. Yan, Z. Wang, and M. Wang, "A fixed-point position observation algorithm and system-on-chip design suitable for sensorless control of high-speed permanent magnet synchronous motor," *Electronics*, vol. 12, no. 14, p. 3160, 2023, https://doi.org/10.3390/electronics12143160.

[57] S. Y. Maddu and N. Ramesh Bhasme, "Performance Analysis of EKF-based Sensorless Induction Motor Drive using FPGA Controller," *2023 13th International Symposium on Advanced Topics in Electrical Engineering*, pp. 1-6, 2023, https://doi.org/10.1109/ATEE58038.2023.10108274.

[58] Y. Gao *et al.*, "Design of position sensorless high-speed PMSM controller based on FPGA," in *IET Conference Proceedings*, vol. 2024, no. 9, 2024, https://doi.org/10.1049/icp.2024.2788.

[59] H. Jiang, L. Zhang and J. Nie, "Design of PMSM Sliding Mode Controller Based on FPGA," *2024 4th Power System and Green Energy Conference (PSGEC)*, pp. 1379-1384, 2024, https://doi.org/10.1109/PSGEC62376.2024.10720973.

[60] B. Sultana, K. Scicluna, J. Attard, C. Seguna and J. Scerri, "Design of a FPGA-based Inverter Drive for HF Injection Based Sensorless Control," *2021 22nd IEEE International Conference on Industrial Technology (ICIT)*, pp. 178-183, 2021, https://doi.org/10.1109/ICIT46573.2021.9453641.